Looking for a simplified approach for the propagation of systematic uncertainty in the motion response of a floater

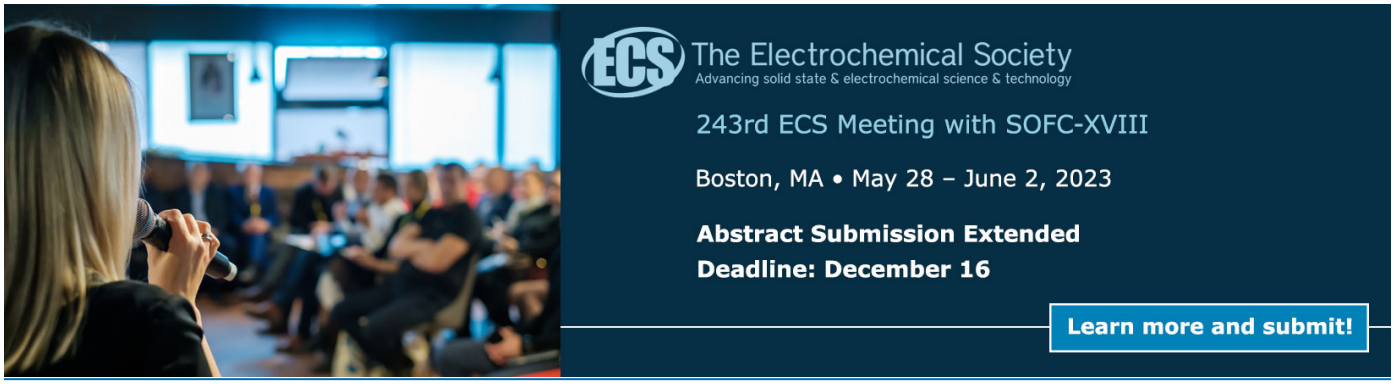

Looking for a simplified approach for the propagation of systematic uncertainty in the motion response of a floater

S. Gueydon, E. Lyden, F. Judge, M. O'Shea and J. Murphy
MaREI Centre, Environmental Research Institute, University College Cork, Cork, Ireland
E-mail: sgueydon@ucc.ie, e.lyden@ucc.ie, frances.judge@ucc.ie, michael.oshea@ucc.ie, jimmy.murphy@ucc.ie

Abstract. This new research considers the 3 main motions of the moored floater (surge, heave and pitch) in head waves and it explores ways to estimate the systematic uncertainties on the RAOs, and 2 other metrics for these signals. Based on linear hydrostatics and the linear potential flow theory, simple relations can be found that bind the main characteristics of a floater. These relations are transformed using linear algebra to express how uncertainty bias on the main characteristics of the tested system can be propagated to the motion responses of the floater. Thanks to this approach, variations of the mooring stiffness, position of the centre of mass, radia of gyration can be represented through simple formulations that allow to very effectively assess their impact of the motion RAOs and other metrics. This approach is verified by comparing simulation and test results of the semisubmersible of the MARINET2 floating wind round robin campaign to approximations deduced from these theoretical relations.

1. Introduction

The present research is motivated by the inter-laboratory comparison of model-tests carried out during the wind round robin testing of MARINET2. However, the concept of uncertainty analysis (UA) in engineering is not specific to model-testing, nor to experimental results but can also be applied to numerical simulations. Including the uncertainty bound in numerical results becomes more and more popular especially as the complexity of these tools increases (e.g. uncertainty in CFD results by [3] and [12]). Following the definition given by the American Society of Mechanical Engineering ([9]), the total uncertainty is a combination of random uncertainty and systematic uncertainty. The random errors can easily be captured by quantifying the dispersion among the results of repeated experiments: the larger the dispersion is, the less precise a measurement is. This is not only due to the intrinsic precision of the measurement device but also caused by the influence of all changes in the test environment and model set-up. Thus, it is interpreted as a random behaviour. On the other hand, the systematic uncertainty is a reflection of how accurately all parameters of the experiment are known. Thus, the analysis of the systematic uncertainty starts by identifying the parameters whose lack of accurate knowledge of may lead to a significant deviation of the experimental results. In the particular context of testing a semisubmersible floating wind turbine in a wave basin, the present study can build upon previous studies done by Robertson ([11]) and Somoano ([13]). Robertson has found that among 24 parameters with significant levels of systematic uncertainty, a small

selection contributes the most to the total systematic uncertainty: the position of the centre of gravity (CoG), the moment of inertia, the stiffness of the mooring system, the diameter of the floater's columns, the draft and the mass of the floater, and the wave amplitude. It is noteworthy that most of these parameters relate to the basic characteristics of the floater. Biases on floater's characteristics are due to the construction of the model, or to the inaccuracy in the measurements of these characteristics. Once that realistic bias on these main parameters are determined, their impact on the responses of the tested specimen must be evaluated. In the current state of the art of UA for hydrodynamic testing, there are no well established methods to carry out this evaluation. Based on a review of recent published works on UA applied to floating wind ([11], [13], [2]), the preferred approach seems to be to propagate bias through numerical simulations. The numerical tools used in these works are time domain simulation tools. The common approach of these works consist in "comparing the platform response of these uncertainty propagations with the ones of the unperturbed simulation as a baseline" ([13]). Although engineering tools (or mid-fidelity according to [8]) are widely used for the loads analysis of FOWTs, these tools still require a large number of input parameters, some of which needs to be calibrated (e.g. damping coefficients, Morison drag and inertia coefficients) in order to obtain reasonable results. Moreover, there are no unique ways of building such a numerical model (even with the same tool) and different approaches can give a significant spreading in their results (e.g. [10]). As a consequence, running many simulations is still a significant investment of time (man and computer) for an accuracy that is sometimes disputable. For instance, Robertson based her assessment of the systematic uncertainty levels on 6 distinct numerical models. All these concerns raises the question of the necessity of employing time domain simulation tools for the propagation of the systematic uncertainty? The research effort of this paper investigates if easier numerical modelling approaches are sufficient to propagate systematic uncertainty.

2. Theoretical background

This section considers several ways of describing the motions of a floating structure in waves. The 6 degrees of freedom (DoF) associated with the floater's motion are 3 translations (1st column) and 3 rotations (2nd column):

- Surge: x
- Sway: y
- Heave: z
- Roll: ϕ
- Pitch: θ
- Yaw: ψ

In this article all data are given at basin's scale. The rotation are expressed in radians (rad) in all equations whereas they are given in degrees (deg) in tables and graphics. A local orthogonal system of axes is defined as drawn in Fig. 1. The x-axis is opposed to the wave direction, the y-axis in pointing towards port-side and the z-axis is vertical upwards. The origin of this system of axes is located underneath the geometrical centre of the hull at its lowest point. The origin is called K for keel. The motions are expressed in this referential that coincides with the floater's initial position (zero tilt and zero trim). Newton's second law can be rewritten in multiple ways leading to different expressions of the motion responses. First, 2 main approaches to assess the motion responses of a moored floater are described. Then variations of these approaches are compared with the aim to find at least one simple method which is still accurate enough to propagate the uncertainty levels on the some of the main characteristics of the floater to its motion responses.

2.1. Equation of floating body motions under the assumption of linear potential flow

Assuming inviscid, incompressible fluid and irrotational flow, the motions of a floating body in waves is given by Equation (1). In linear potential theory, the velocity potential and fluid pressure on the submerged surface of a body are solved using the boundary element method

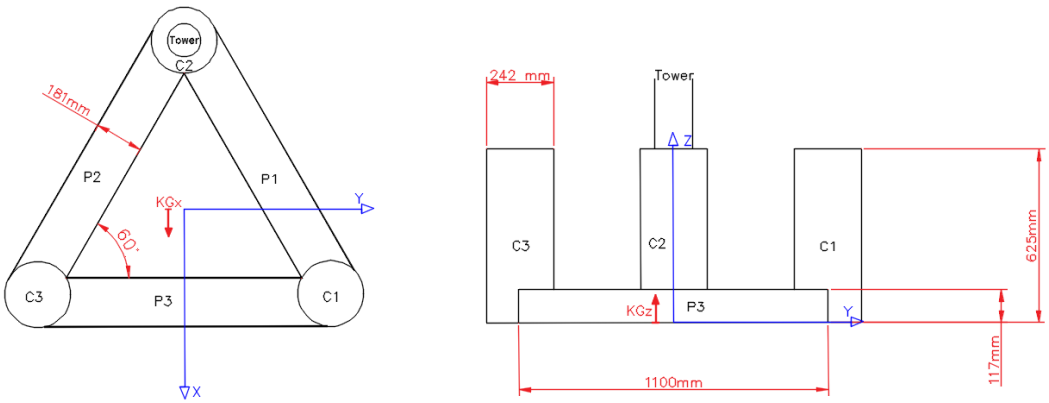

Figure 1. Layout and dimensions of the $1/60^{th}$ scale model of the MARINET2 round robin testing

(BEM). Separate solutions are carried out simultaneously for the diffraction problem, giving the effects of incident waves on the body, and the radiation problem, giving the effects of the motion of the body for each of the prescribed modes of motion. For small motions, the added-mass, the potential damping and the hydrostatic stiffness terms depend exclusively on the submerged geometry. Additionally, the wave loads are also following from the knowledge of the submerged geometry when small wave amplitudes are considered. In other words, varying the location of the centre of gravity (CoG) and the mass distribution (I in (1)) has no impact on all other terms of (1); excepted that the equation needs to be rewritten at the new CoG location.

$$(I + A).\ddot{X} + B_p.\dot{X} + C.X = F \tag{1}$$

where,
X = 6 DoF motion vector at CoG (surge, sway, heave, roll, pitch, yaw);
$\dot{X}$ = 6 DoF velocity vector at CoG (surge, sway, heave, roll, pitch, yaw);
$\ddot{X}$ = 6 DoF acceleration vector at CoG (surge, sway, heave, roll, pitch, yaw);
I = (dry) inertia 6x6 matrix;
A = added-mass 6x6 matrix, which is frequency dependent;
B_p = potential damping 6x6 matrix, which is frequency dependent;
C = hydrostatic 6x6 matrix;
F = wave excitation 6 component vector (surge, sway, heave, roll, pitch, yaw).

For the particular case of a moored floater which experienced some viscous damping, new terms can be added to Equation (1) without compromising its linearity:

- a linear viscous damping B_v can be added to the potential damping B_p,
- a linear mooring stiffness K can be added to the hydrostatic stiffness C.

Equation (1) becomes equation (2) for a moored floater.

$$(I + A).\ddot{X} + (B_p + B_v).\dot{X} + (C + K).X = F \tag{2}$$

If the CoG location is modified then Equation (2) needs to be transferred to the new CoG location. Appendix A gives all details of how this transfer is done. Such that the more generic linear equation (3) can be kept for the rest of the demonstration.

$$(I_G + A_G).\ddot{X} + B_G.\dot{X} + C_G.X = F_G \tag{3}$$

where,
B_G is the total damping at CoG;
C_G is the total stiffness at CoG.

If an harmonic excitation is applied to this linear system then the motions will also be harmonic.

$$F_G = F_\omega * exp(k.X_0 + \phi - j * \omega.t), \quad X_G = X_\omega * exp(k.X_0 + \beta - j * \omega.t).$$

where,
ω = frequency of a single harmonic wave;
F_G = wave excitation at the centre of gravity for frequency ω;
F_ω = wave excitation amplitude coefficient at frequency ω;
ϕ = wave excitation phase value at frequency ω;
k = wave number for frequency ω;
X_0 = initial values of position vector;
j = imaginary unit number ($j = \sqrt{(-1)}$);
X_ω = motion amplitude coefficient at frequency ω;
β = phase value of the motion response at frequency ω.

As we are uniquely interested in the motion amplitude, we deliberately leave any phase information aside:

$$F_G = F_\omega * exp(-j * \omega.t), \quad X_G = X_\omega * exp(-j * \omega.t).$$

Equation (3) defines a linear relation between the wave loading and the motion responses for every frequency:

$$(-\omega^2.(I_G + A_G) - j * \omega.B_G + C_G) * X_\omega = F_\omega \tag{4}$$

Equation (4) constitutes a system of 6 equations with 6 unknown variables (one per DoF) for every frequency. This system of equations can be inversed all at once, such that the couplings between DoFs are accounted for. For every frequency, the solution is a series of complex numbers which amplitudes are the motion RAO coefficients. Otherwise, it can be simplified by keeping only the diagonal terms of $I_G + A_G$, B_G and C_G and zeroing all cross terms (which comes down to neglecting any coupling between DoFs). In the latter case, there is an algebric solution to this simplification of equation (3) for each k^{th}-DoF:

$$X_{\omega_k} = \frac{F_{\omega_k}}{\sqrt{(-\omega^2.(I_{G_{kk}} + A_{G_{kk}}) + C_{G_{kk}})^2 + (\omega.B_{G_{kk}}.)^2}} \tag{5}$$

The algebric expression in (5) is a simple formula that estimates the motion RAO amplitude for a single DoF (k) for every frequency (ω).

The eigen modes of the system are found by solving Equation (4) when the damping and the right hand side are forced to zero (see Appendix B for more details). The eigen modes are usually made of a combination of several DoFs due to the influence of the coupling terms in $I_G + A_G$ and C_G. There again, these couplings between DoFs can be ignored by zeroing all crossing terms. The solution will then be eigen frequencies (or natural periods) for the 6 independent DoFs: surge, sway, heave, roll, pitch and yaw. These periods should be similar to the natural period determined from the decay tests in each respective DoF. For levels of damping that are far below the critical damping, the natural period of the k^{th}-DoF can be written as:

$$T_k = 2.\pi.\sqrt{\frac{(I_{G_{kk}} + A_{G_{kk}})}{C_{G_{kk}}}} \tag{6}$$

For a moored floater considered as a rigid-body with weak coupling between DoFs, the 2 equations (5) and (6) make 2 first-hand approximations of its responses to waves and its natural periods that will appear very handy while doing an uncertainty analysis.

2.2. Equation of motion as a system of differential equations

The motions of a floating body in waves can be modelled by using Cummin's Equation ([1]) as follows:

$$\sum_{l=1}^{6}(I_{kl}+A_{kl}^{\infty}).\ddot{X}_l+\int_{-\infty}^{t}\kappa_{kl}(t-\tau).\dot{X}_l(\tau).d\tau+C_{kl}.X_l=F_k(t) \tag{7}$$

where,
X_l = motion at CoG for l^{th} DoF (l=1 for surge, l=6 for yaw);
$\dot{X}_l$ = velocity at CoG for l^{th} DoF (l=1 for surge,..., l=6 for yaw);
$\ddot{X}_l$ = acceleration at CoG for l^{th} DoF (l=1 for surge,..., l=6 for yaw);
F_k = wave excitation load at CoG for l^{th} DoF (l=1 for surge,..., l=6 for yaw);
I_{kl} = element of inertia matrix for k^{th} row and l^{th} column;
C_{kl} = element of hydrostatic stiffness matrix for k^{th} row and l^{th} column;
A_{kl}^{∞} = element of added mass matrix for infinite frequency for k^{th} row and l^{th} column;
κ_{kl} = element of impulse response function matrix for k^{th} row and l^{th} column;

A_{kl}^{∞} and κ_{kl} are directly linked to the potential damping B_p of Equation (1) by the following relations:

$$A_{kl}^{\infty}=A_{kl}(\omega)+\frac{1}{\omega}*\int_{0}^{+\infty}\kappa_{kl}(\tau).sin(\omega t).d\tau \tag{8}$$

$$\kappa_{kl}(t)=\frac{2}{\pi}*\int_{0}^{+\infty}B_{p_{kl}}(\omega).cos(\omega t).d\omega \tag{9}$$

Cummins equation for ship motion can be used to model the motion of a moored floater in waves. This can be done by adding a mooring stiffness to the hydrostatic stiffness of C_{kl} like previously done in Equation (2). Nevertheless, it is also possible to include non-linear mooring loads by including mooring loads to the right hand side of Equation (7). These two options are also available for the inclusion of viscous damping too. In fact, Equation (2) allows for the inclusion of any non-linear loads, like higher order wave loads, which makes it much more realistic than Equation (2) of the previous section. Being a system of ordinary differential equations (ODE), Equation (2) is solved numerically by integration using for instance Runge-Kutta methods. Many commercial engineering tools have this functionality (e.g. ANSYS AQWA, Orcaflex). For the present study an internal research tool has been used. The results of this process are time series of the motions for 6 DoFs.

Through post-processing analysis, the RAOs of the motion can be determined. These RAOs are taken as reference as the numerical model is more capable of capturing the main physics leading the response of the platform. For instance, the motions resulting from the numerical ODE model of the present study include both first and second order difference frequency wave loading, the mooring lines are modelled individually as spring-lines, the equivalent linear damping is calibrated from experimental decay tests.

2.3. Synopsis

When the moored floater is considered as a linear mass-spring-damper system, the natural periods can be estimated by (6) ignoring any coupling between DoFs. In addition, the

motion RAOs can be easily estimated in frequency domain and variations of some mechanical characteristics of the system can be propagated to the motion RAOs.

Equation (A.2) is providing us with the mean to vary basic properties of the floater as long as the submerged geometry remains the same. The following parameters can be changed:

- the position of the CoG (KG),
- the inertia moments contained in the sub-matrix $I_{4..6,4..6}$,
- terms of the hydrostatic stiffness $C_{4..6,4..6}$ that depend on KG or the inertia moments,
- the mooring stiffness K can be modified.

The solutions of the system of equations presented in (3) are the motion RAOs that account for possible coupling between DoFs. When coupling between DoFs are neglected, each independent motion RAO can be approximated by the simple formula conforming to (5). In parallel, a more sophisticated approach can be followed. This consists in solving the Cummin's Equation (7) in time domain. Note that this time domain approach is commonly implemented in mid-fidelity (or engineering) tools like OpenFAST. This approach offers the possibility of accounting for more effects that can alter the motion responses, like:

- more realistic description of the mooring system (i.e. modelling of the mooring lines),
- inclusion of non-linear damping (e.g. quadratic damping or Morison drag loads),
- second-order wave loads.

As this latter approach is more complete than the simplified frequency domain approaches, it will serve as a reference for the evaluation of all other approximations (i.e. different ways to solve the equations of motion in frequency domain). Finding the motion RAOs in frequency domain like in the first approach is more direct than simulating the motions in time-domain and subsequently determining the RAOs by post-processing like in the second approach.

3. Propagation of systematic uncertainties

The question that this paper attempts to answer is: which degree of complexity is necessary to propagate bias on some key parameters to RAO's and other metrics used for the analysis of model-tests?

To this end, RAOs and 2 other metrics utilized in the wind round robin basin tests of a semisubmersible floating wind turbine ([4]) will be compared following the approaches of the previous section.

This comparison has been done for a few irregular waves of the wind round robin test plan (given in Table 1). For practical reasons, the tests in irregular waves are analyzed on a fixed range of frequencies $[f_1, f_2]$. This range of frequency is chosen as a function of the considered theoretical spectrum and also the capacities of the wave maker. Gueydon et Al ([5]) discusses how each of these waves are likely to excite the model based on their power spectral densities and the associated group power spectral contents.

This paper uses two metrics which have been introduced by Gueydon et Al in [4]. The metric used to examine the response of the system in the wave frequency range, M_{WF} is calculated from

$$M_{WF} = \sqrt{\frac{\int_{f_1}^{f_2} S_{signal}\, df}{\int_{f_1}^{f_2} S_\eta\, df}}, \tag{10}$$

where:
S_{signal} is the PSD of the signal (surge, heave or pitch),
S_η is the wave power spectrum,
$[f_1, f_2]$ (Hz) is the wave frequency range considered for the analysis.

Table 1. Expected resonance responses for irregular wave conditions (low frequency (LF) or wave frequency (WF)) and WF range [f_1,f_2] (Hz) per wave condition

Motion mode	**Surge**	**Heave**	**Pitch**	f_1 **(Hz)**	f_2 **(Hz)**
JONSWAP $T_p = 1.29\ s$	LF	LF	LF	0.50	1.3
JONSWAP $T_p = 1.81\ s$	LF	WF	LF	0.35	1.2
JONSWAP $T_p = 2.58\ s$	LF	WF	WF	0.25	1.2
Pink-Noise	LF	WF	WF	0.25	1.2

The metric T_r gives an estimate of the period of the resonance response:

$$T_r = \frac{\int_{f_e-\delta f}^{f_e+\delta f} S_{signal}^4 \, df}{\int_{f_e-\delta f}^{f_e+\delta f} f \cdot S_{signal}^4 \, df}. \tag{11}$$

Where:
S_{signal} is the PSD of the signal (surge, heave or pitch),
f_e is its main resonance frequency and δf is a frequency band around f_e that covers the peak shaped resonance response of the signal. The natural periods measured during decay tests are used for f_e ([4]).

On top of the 3 ways to estimate the RAOs presented in the previous section, an additional way is suggested. Having a formula to estimate the RAOs opens up the possibility to easily optimized some of its parameters to better match the reference case. An optimization parameter α is added to the formula (3). This parameter acknowledges the fact that the level of damping in waves is not always known. The linear damping B_v of (1) is usually determined from the analysis of decay tests in still water. For the subject of this study, previous publications have reported that the damping is mainly quadratic for surge, heave and pitch ([5]). Such that B_v alone would not be enough to represent the total damping acting on the semisubmersible in waves. In the new formula (12), α represents the equivalent linear damping added to the system to best fit the metric M_{WF} of the reference case in the considered seastate. An optimization scheme delivers the value of α for each DoF. In this approach, coupling between DoFs are ignored.

$$X_{\omega_k} = \frac{F_{\omega_k}}{\sqrt{(-\omega^2.(I_{G_{kk}} + A_{G_{kk}}) + C_{G_{kk}})^2 + \omega^2 * (B_{G_{kk}} + \alpha)^2}}; \tag{12}$$

Finally, 4 different ways to estimate the motion RAOs and the metrics M_{WF} are compared:

- 'LSE' is the approach solver the linear system of equation (LSE) (2),
- 'Formula' is the approach based on the formula (5) (relying on non-optimized output data of the potential flow solver),
- 'Fit' is the approach based on the optimization of the linear damping in the formula (12),
- 'ODE' is the approach which calculate RAO's from the time domain solution of equation (7).

The 3 first approaches can be classified as "low-fidelity" whereas the last one uses a "mid-fidelity" simulation tool ([8]).

The evolution of these metrics under the variations of the diverse key parameters can be studied:

(i) the mooring stiffness in surge K_{11},

(ii) the vertical position of the CoG KG_z,
(iii) the radius of gyration around pitch R_{55}.

This can easily be done in a numerical study for which individual parameters (such as K_{11}, KG_z and R_{55}) can be varied independently from the others. In that case, the results of a time domain simulation (i.e. ODE) constitutes the reference set to which the approximations (LSE, Formula and Fit) are compared to. Such comparison has been carried out as part of this research. It has confirmed the excellent resemblance of RAO's obtained by these 4 different approaches. Differences were only noticed around the resonance peaks when those are inside the wave frequency range ($[f_1, f_2]$ of Table 1). For the conciseness of this paper, no results of this numerical study are presented here. Instead, another variation which combines changes in KG_z and R_{55} is further developed in the next section. The availability of experimental results for this variation motivated this choice.

4. Demonstration and validation against model-tests

In April 2021, UCC has executed an additional campaign of model-tests during which some properties of the physical model were voluntary varied. This test campaign is reported by Lyden ([7]). One of these variations consisted in shifting some mass from the nacelle to the top of the 3 columns. Distributing some of the nacelle mass among the 3 columns is a way to change the position of the CoG and the inertia moments of the floating platform. 3 systems were tested in the pink-noise waves of Table 1):

- System O: The system with its original mass distribution (5 repeats),
- System A: a system in which 1200g of the nacelle was replaced by 400 g of lead on top of each of the 3 column (4 repeats),
- System B: a system in which 1500g of the nacelle was replaced by 500 g of led on top of each of the 3 column (5 repeats).

Care was taken to keep the equilibrium trim and tilt angle of all systems as small as possible, such that the submerged geometry remains the same for O, A and B. The mooring was identical and conform to the description of the original test set-up ([5]). These experiments provides us with data that can be used to calculate the metrics T_r and M_{WF} for 3 distinct mass distributions of the moored submersible platform.

To complement the experimental data, a numerical study was run in which the shifting of mass between the nacelle and the 3 columns was modelled in more and smaller steps than during the experiments. 13 cases were simulated:

- Negative mass shift: 6 steps in which mass was taken off from the columns and put on the nacelle (i.e. -3*100g, -3*200g, -3*300g, -3*400g, -3*500g, -6*600g),
- System O: The system with its original mass distribution (i.e. 0g shifted),
- Positive mass shift: 6 steps in which mass was taken off from the nacelle and put on top of the columns (i.e. 3*100g, 3*200g, 3*300g, 3*400g, 3*500g, 6*600g).

For each mass shift, the corresponding variations of KG_z and R_{55} need to be calculated before they can be propagated in the formulae (LSE, Formula, Fit) and the numerical model (ODE) for the 4 approaches. As the results of these variations, values of KG_z lie in a range of $\pm 15(\%)$ of the original value (O) while R_{55} belongs to a range of $\pm 30(\%)$.

The demonstration of the method is done with the pink-noise irregular waves of the wind round robin test plan (given in Table 1). Thanks to its broad wave frequency range, the pink-noise gives RAOs with the largest frequency range from all waves. The heave and pitch resonance frequencies are directly excited by the wave energy of this sea-state. This wave was run in the basin for 1860 s.

First, the approximations (LSE, Formula and Fit) are directly compared to test results of the original system exposed to the pink-wave. Figure 2 displays the motion RAOs. The RAOs are plotted on three rows: surge on the top row, heave on the middle row and pitch on the bottom row. While the RAOs for the test are obtained from the analysis of the recorded motions and wave elevation, the other 3 approximations are directly deduced in frequency domain from Equations (4), (5) and (12). On the one hand, the global shape of the RAOs are similar, with resonance peaks approximately located at the same frequencies. On the other, there are many differences. The surge RAO of the test results is dented for frequencies below 0.8 Hz whereas the approximated surge RAOs are smooth. It has been shown that these irregularities in the surge RAO of the test data are caused by wave reflection in the basin ([5]). The shape and the magnitudes of the resonance peaks in heave and pitch for the test data look very different for the approximations. Non-linear effects are amplified at resonance in real life. The resonance responses in heave and pitch have been shown to be non-linear for this system ([5], [4]). The theoretical approach upon which the approximations are based does not account of any basin effect (i.e. reflection). Moreover, the approximations are fully linear and account exclusively for a linear damping. The RAOs of the 'Fit' approximation is calculated using a linear damping coefficient that has been optimized to match the M_{WF} of the test data. In heave, this RAO is higher than the RAOs of other approximations ('LSE' and 'Formula'). In pitch this is the other way round, the 'Fit' RAO is smaller than the RAOs of 'LSE' and 'Formula'. The peak of the 'Fit' RAO in pitch is smaller and broader than for the pitch RAO of the test. In heave and pitch, the correspondance between all RAOs is stronger for frequencies well above the respective resonance frequencies. This illustrates the specific challenges of approximating the RAOs around the resonance peaks.

Secondly, the metrics T_r and M_{WF} of the approximations are compared to the results of a numerical model (ODE). The numerical simulations were run in an R&D software for a duration corresponding to the test duration. Actually, the wave elevation measured during the calibration of these model-tests was scaled-up and used as input wave for the simulations (run at full scale). The numerical model used 3 horizontal spring lines for the mooring system conform to the description of the model-test set-up ([5]). In order to keep the response of the model as linear as possible, linear damping coefficients were used. The damping B_v was calibrated using decay tests in still water for LSE, Formula and Fit. In the Fit approximation, the linear damping α is added on top of B_v to obtain matching M_{WF} for Fit and the reference case (ODE). The hydrodynamic input data characterizing the floater come from a linear potential flow calculation extended to the second-order for the low frequency wave loads. First and second-order wave loads were accounted for in the simulations. The inertia matrix, the added-mass, the potential damping and first-order wave loads are shared input data between the 4 approaches (ODE & the 3 approximations: LSE, Formula and Fit). While the actual mooring loads are calculated based on the position of the floater in the simulation (ODE), the approximations used an equivalent mooring stiffness. In all cases, the equilibirum between the weight and the buoyancy loads is based on the linear expression of the hydrostatic matrix ([6]). Figure 3 gives an overview of the process leading to the comparison of the metrics T_r and M_{WF} in this numerical study.

Thirdly, the evolution of the metrics T_r and M_{WF} for every method are compared to each other. The metrics resulting from the tests are displayed on the same figures using diamond symbols.

The variations of the metrics are plotted with 3 graphics on top of each other: surge being on top, heave being in the middle and pitch being at the bottom. Figure 6 gives the variations of T_r when the mass distribution varies. T_r varies mainly for surge. The evolution of M_{WF} is shown in Figure 7. The effect of variation of the mass distribution is small for surge and heave whereas it is large in pitch. Although there are differences in the estimates of T_r and M_{WF} depending on the followed approximation (LSE, Formula, Fit), all trends with regards

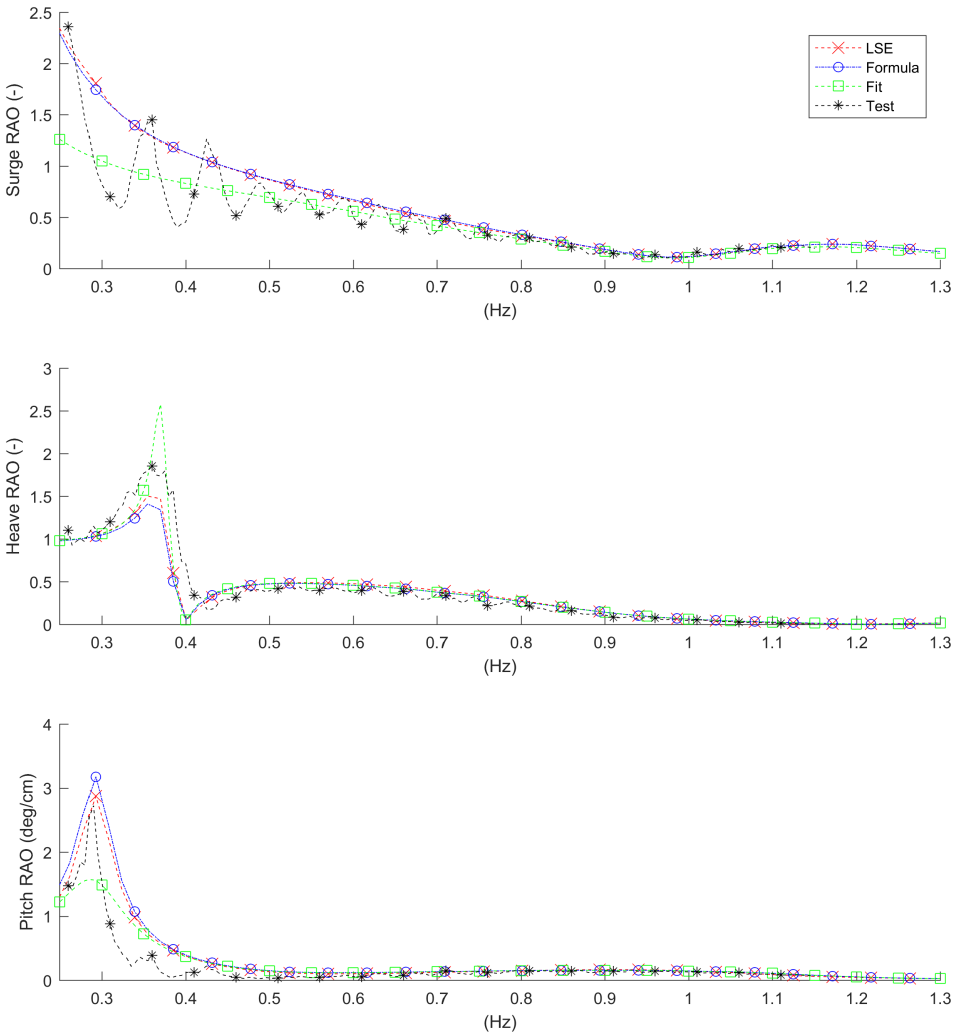

Figure 2. Motion RAOs of original system calculated following 3 approximations versus test results in the 'Pink-Noise' wave of Table 1

to the variation of the mass distribution are the same whatever the approach is. Focusing on the metrics in pitch which are the most impacted by the considered variation, the numerical results ODE agree reasonably well with the experimental data (Test). Figure 7 also shows that the approximation of M_{WF} based on the fitted formula (Fit) of Eq. (12) gives values that are equivalent to the simulations and the model-tests. This demonstrates that simple formulae can accurately predict the evolution of these metrics.

Even if the proposed approximations don't reproduce perfectly the results of model-tests (Figure 2), they are able to capture the evolution of the motion RAOs and metrics M_{WF} and T_r with a good accuracy for a very low computational cost. It is thereby justified to use these formulae for the propagation of the uncertainties on some of the design parameters of the physical

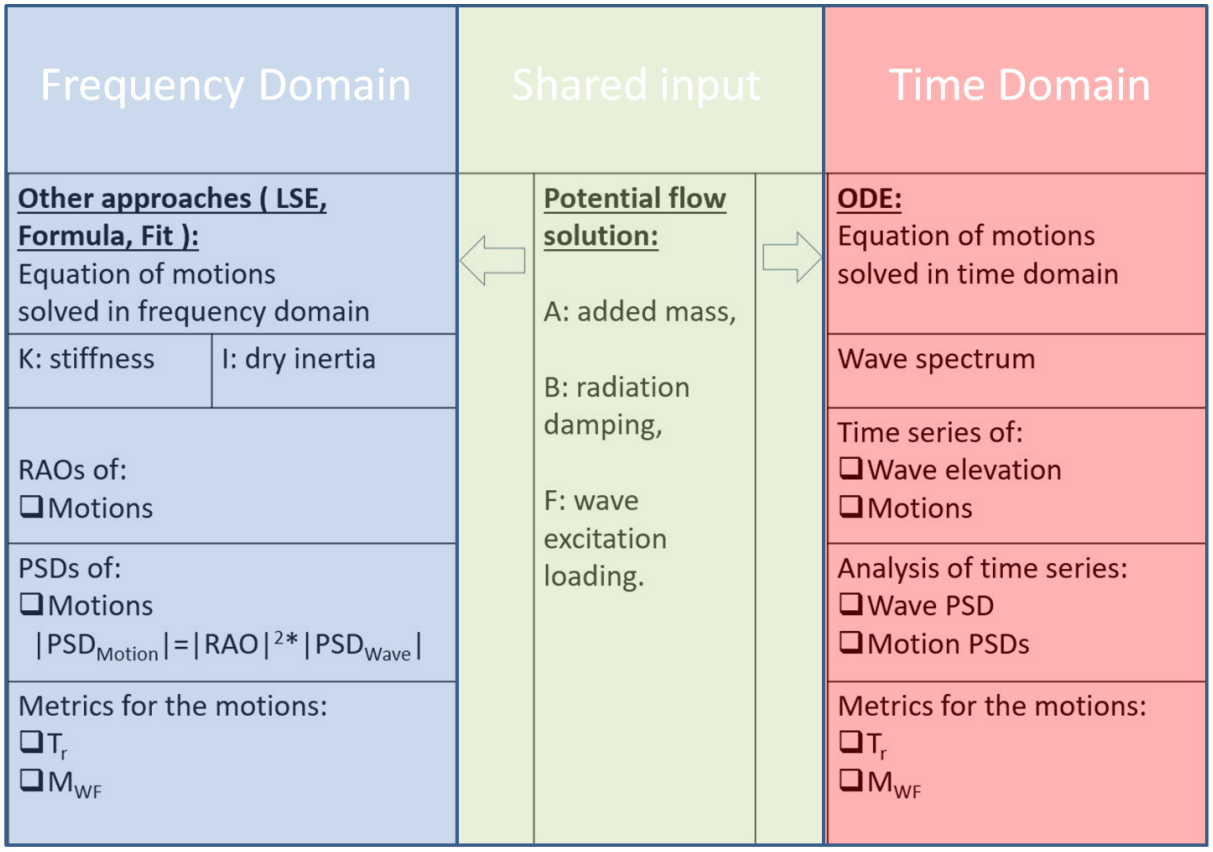

Figure 3. Overview of the process for the comparison of the different approaches

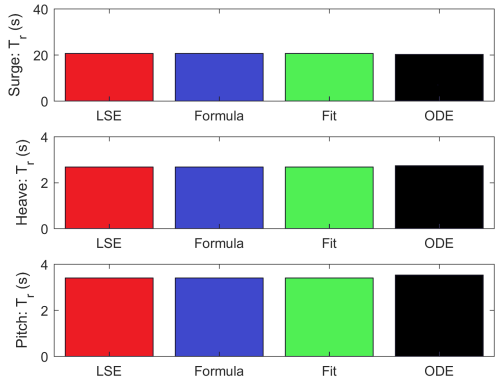

Figure 4. Metrics T_r of original system calculated following 4 different approaches.

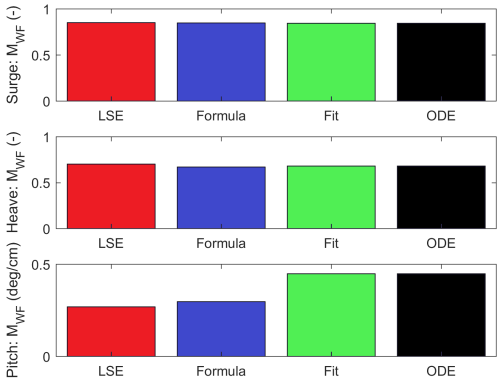

Figure 5. Metrics M_{WF} of original system calculated following 4 different approaches.

model.

5. Conclusions

This paper follows up the introduction of metrics T_r and M_{WF} describing the response of the moored semisubmersible floating wind turbine tested during the wind round robin campaign

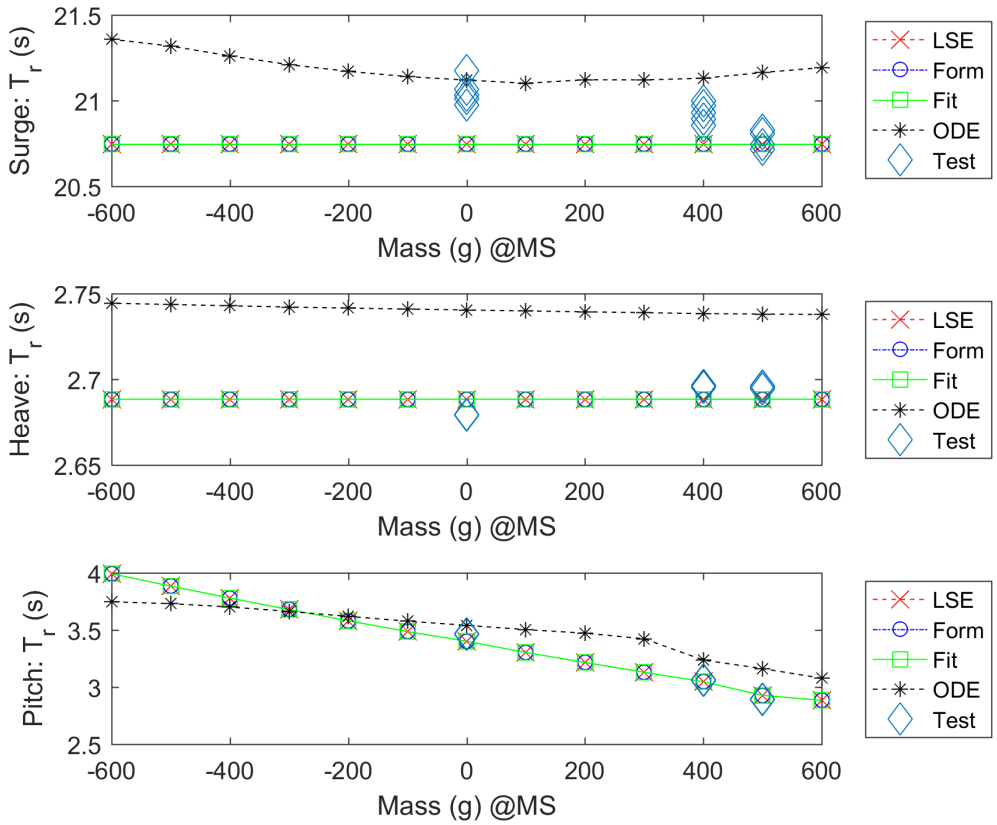

Figure 6. Evolution of metrics T_r when weights are shifted between the nacelle and the top of the 3 columns.

of the Horizon2020 MARINET2 project ([4]). It demonstrates that simple formulae derived from linear hydrostatics and the equation of motion can be used to represent the evolution of these two metrics when the mass distribution varies. This shows that such approximations are sufficient to accurately predict the evolution of the motion responses under the variations of some main characteristics of the tested system (like the position of the CoG, the inertia moments, stiffness of the mooring system). This finding can be used for the assessment of the level of uncertainties inherent to these main characteristics. Any impact on the motion responses caused by a bias on the position of the CoG, the inertia moments, the stiffness of the mooring system can be predicted using these approximations. These approximations require only the potential flow solution of the system and overall characteristics which are usually determined prior to or during the test campaign: global stiffness coefficients, estimated position of the CoG and inertia moments. With these input data, the impact of any variation of the main parameters of the system can be determined instantly using these approximations. Considering how much more efficient these formulations are compared to time domain simulations of common engineering tools, the authors propose to use these formulations for the uncertainty analysis of the floating wind semisubmersible of the round robin testing of MARINET2. The authors believe that these approximations can be applied to propagate uncertainty levels on the motions of any floater as long as it fulfills 3 main conditions:

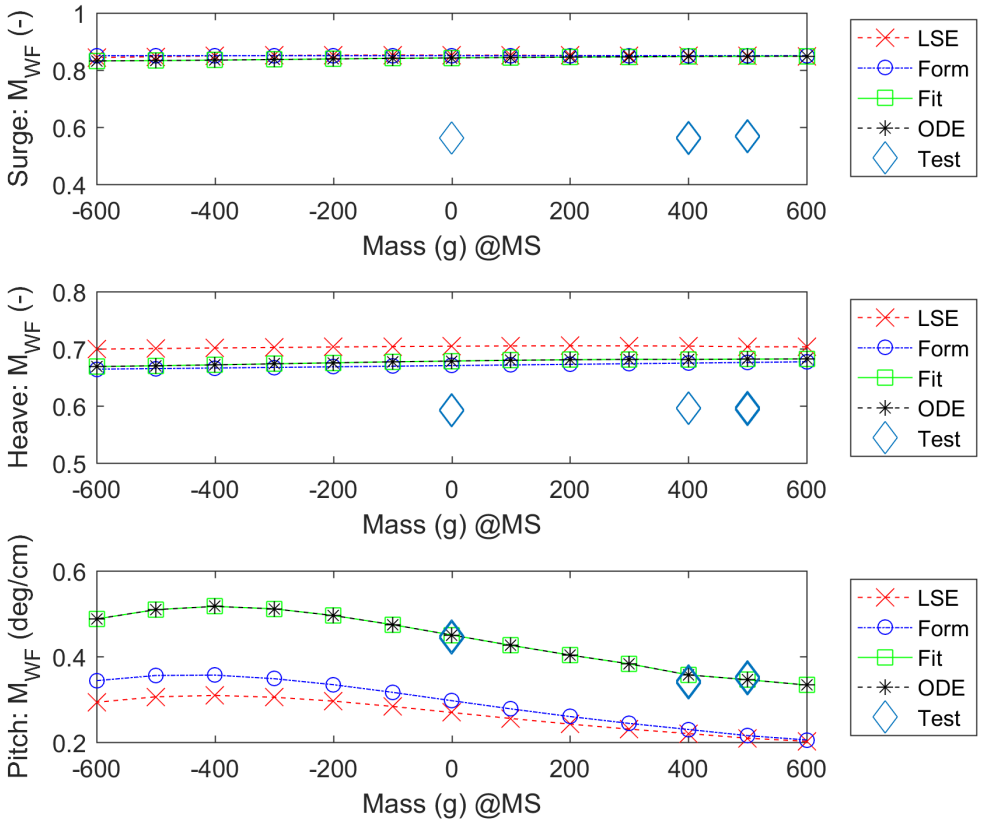

Figure 7. Evolution of metrics M_{WF} when weights are shifted between the nacelle and the top of the 3 columns.

(i) its motion can be reasonably well predicted by the linear potential flow theory,
(ii) it behaves like a rigid body,
(iii) the considered DoFs are weakly coupled.

The first condition exclude any metric that would represent the amplitude of the low frequency motion of a moored floater (e.g. the amplitude of the low frequency surge motion response). Further research is require to derive formulae that capture the motion outside the wave frequency range (i.e. the low and the high frequency non-linear responses).

6. Acknowledgments

6.1. Author contributions

Conceptualization, S.G; **methodology**, S.G.; **formal analysis**, S.G.; **investigation**, E.L.; data curation, E.L., M.L.B; **writing—original draft preparation**, S.G.; **writing—review and editing**, F.J.; **visualization**, S.G.; **project administration**, M.O.S., J.M.; **funding acquisition**, J.M.; **supervision**, J.M.
All authors have read and agreed to the published version of the manuscript.

6.2. funding
This research was funded by European Union's Horizon 2020 research and innovation programme under grant agreement number 731084, project MaRINET2 (Marine Renewable Infrastructure Network for Enhancing Technologies 2).

7. Abbreviations

The following abbreviations are used in this manuscript:

CoG	Centre of Gravity
DoF	Degree of Freedom
FOWT	Floating Offshore Wind Turbine
ITTC	International Towing Tank Conference
JONSWAP	Joint North Sea Wave Project
LF	Low Frequency
PSD	Power Spectral Density
RAO	Response Amplitude Operator
WF	Wave Frequency

8. References

[1] WE Cummins. The impulse response function and ship motions, 1962. Internal report.
[2] Cian J. Desmond, Jan-Christoph Hinrichs, and Jimmy Murphy. Uncertainty in the physical testing of floating wind energy platforms' accuracy versus precision. *Energies*, 12(3), 2019.
[3] Luís Eça and Martin Hoekstra. Discretization uncertainty estimation based on a least squares version of the grid convergence index. In *Proceedings of 2nd Workshop on CFD Uncertainty Analysis*, 01 2006.
[4] Sebastien Gueydon, Frances Judge, Eoin Lyden, Michael O'Shea, Florent Thiebaut, Marc Le Boulluec, Julien Caverne, Jérémy Ohana, Benjamin Bouscasse, Shinwoong Kim, Sandy Day, Saishuai Dai, and Jimmy Murphy. A heuristic approach for inter-facility comparison of results from round robin testing of a floating wind turbine in irregular waves. *Journal of Marine Science and Engineering*, 9(9), 2021.
[5] Sebastien Gueydon, Frances M Judge, Michael O'Shea, Eoin Lyden, Marc Le Boulluec, Julien Caverne, Jérémy Ohana, Shinwoong Kim, Benjamin Bouscasse, Florent Thiebaut, Sandy Day, Saishuai Dai, and Jimmy Murphy. Round robin laboratory testing of a scaled 10 mw floating horizontal axis wind turbine. *Journal of Marine Science and Engineering*, 9(9), 2021.
[6] JMJ Journee and WW Massie. *Offshore Hydromechanics*. Delft University of Technology, 2001.
[7] Eoin Lyden, Frances Judge, Sebastien Gueydon, Michael O'Shea, and Jimmy Murphy. An experimental investigation into the most prominent sources of uncertainty in wave tank testing of floating offshore wind turbines. *draft paper submitted to Journal of Physics: Conference Series*, fev 2022.
[8] Aldert Otter, Jimmy Murphy, Vikram Pakrashi, Amy Robertson, and Cian Desmond. A review of modelling techniques for floating offshore wind turbines. *Wind Energy*, 12 2021.
[9] ASME PTC19.1. *Test Uncertainty, Performance Test Codes*. American Society of Mechanical Engineers, 3 edition, 2018.
[10] A N Robertson, S Gueydon, E Bachynski, L Wang, J Jonkman, D Alarcón, E Amet, A Beardsell, P Bonnet, B Boudet, C Brun, Z Chen, M Féron, D Forbush, C Galinos, J Galvan, P Gilbert, J Gómez, V Harnois, F Haudin, Z Hu, J Le Dreff, M Leimeister, F Lemmer, H Li, G Mckinnon, I Mendikoa, A Moghtadaei, S Netzband, S Oh, A Pegalajar-Jurado, M Q Nguyen, K Ruehl, P Schünemann, W Shi, H Shin, Y Si, F Surmont, P Trubat, J Qwist, and S Wohlfahrt-Laymann. OC6 phase i: Investigating the underprediction of low-frequency hydrodynamic loads and responses of a floating wind turbine. *Journal of Physics: Conference Series*, 1618(3):032033, sep 2020.
[11] Amy Robertson, Erin E. Bachynski, Sebastien Gueydon, Fabian Wendt, and Paul Schünemann. Total experimental uncertainty in hydrodynamic testing of a semisubmersible wind turbine, considering numerical propagation of systematic uncertainty. *Ocean Engineering*, 195:106605, 2020.
[12] Monica Silva, Marcelo Vitola, Luís Eça, Paulo Esperança, and Sergio Sphaier. Numerical uncertainty analysis in regular wave modeling. *Journal of Offshore Mechanics and Arctic Engineering*, 140, 02 2018.
[13] Miguel Somoano, Tommaso Battistella, Sergio Fernández-Ruano, and Raúl Guanche. Uncertainties assessment in real-time hybrid model for ocean basin testing of a floating offshore wind turbine. *Journal of Physics: Conference Series*, 2018(1):012036, sep 2021.

Appendix A. Transfer of the equation of motions from H to G

Let's take $\overrightarrow{KH}$ the position vector of the original point where the potential flow solver has solved equation (1) (i.e. where A, B_p and C are known) and write down this equation at a new centre of mass with location $\overrightarrow{KG}$.

$$\overrightarrow{HG} = \begin{bmatrix} \Delta x \\ \Delta y \\ \Delta z \end{bmatrix}$$

The forces applied at H come with additional moments when they are expressed at G.

$$\begin{bmatrix} \overrightarrow{F} \\ \overrightarrow{M_G} \end{bmatrix} = \begin{bmatrix} \vec{F} \\ \overrightarrow{M_H} + \overrightarrow{GH} \times \overrightarrow{F} \end{bmatrix}$$

This transfer of loads can be rewritten in matrix form. Defining 6 component vectors for the loads with the forces in the first 3 rows (along the axes x, y and z) and the moment (around the axes x, y and z), the relation for the transfer of the loads between H and G becomes:

$$\begin{bmatrix} F_x \\ F_y \\ F_z \\ M_{xG} \\ M_{yG} \\ M_{zG} \end{bmatrix} = P. \begin{bmatrix} F_x \\ F_y \\ F_z \\ M_{xH} \\ M_{yH} \\ M_{zH} \end{bmatrix}$$

with

$$P = \begin{bmatrix} 1 & 0 & 0 & 0 & 0 & 0 \\ 0 & 1 & 0 & 0 & 0 & 0 \\ 0 & 0 & 1 & 0 & 0 & 0 \\ 0 & \Delta z & -\Delta y & 0 & 0 & 0 \\ -\Delta z & 0 & \Delta x & 0 & 0 & 0 \\ \Delta y & -\Delta x & 0 & 0 & 0 & 0 \end{bmatrix}$$

The transformation matrix P has the handy property of being orthogonal and therefore P^{-1} is equal to P^T.

The motion at H is expressed in a 6 component vector with the translations in the first 3 rows (surge, sway and heave) and the rotations (in rad) in the last 3 rows (roll, pitch and yaw):

$$\overrightarrow{X_H} = \begin{bmatrix} x \\ y \\ z \\ \phi \\ \theta \\ \psi \end{bmatrix}$$

"For small angles, the transformation matrix from the body-bound coordinate system to the steadily translating coordinate system is very simple" (dixit Journee in [6], section 6.2.5). Motions at the new CoG ($\overrightarrow{KG}$) are obtained from the motions at the point H ($\overrightarrow{KH}$) by the following linear relations:

$$\begin{aligned} x_G &= x - \Delta y.\psi + \Delta z.\theta \\ y_G &= y + \Delta x.\psi - \Delta z.\phi \\ z_G &= z - \Delta x.\theta + \Delta y.\phi \end{aligned}$$

These relations can be written in matrix form using the same transformation matrix P:

$$\overrightarrow{X_G} = P^T.\overrightarrow{X_H}; \tag{A.1}$$

For small harmonic motions, the matrix relation A.1 is also valid to link velocities and accelerations at G and H. And finally the equation of motions (2) can be fully rewritten at G in Equation (A.2).

$$P.(I+A).P^{-1}.\ddot{X_G} + P.(B_p+B_v).P^{-1}.\dot{X_G} + P.(C+K).P^{-1}.X_G = P.F_H \tag{A.2}$$

where,
I, A, B_p and C are still quantities that are valid at the location H where the potential flow solver was run. B_v and K were also originally defined at H. All these terms are simply transferred to a new location G. Equations (1) and (A.2) are basically the same; only each of the terms of (1) has been replaced by a new expression:

- the inertia is replaced by the inertia at G: $I_G + A_G = P.(I+A).P^T$,
- the total damping is replaced by the damping at G: $B_G = P.(B_p+B_v).P^T$,
- the total stiffness is replaced by the stiffness at G: $C_G = P.(C+K).P^T$,
- the forcing term is replaced by loads transferred at G: $F_G = P.F$.

Appendix B. Eigen frequencies

The eigen modes of the system are solutions of Equation (4) when the excitation and damping terms are not considered:

$$(-\omega^2.(I_G + A_G) + C_G) * X_\omega = 0 \tag{B.1}$$

For harmonic motion Equation (B.1) can be rewritten in:

$$((I_G + A_G)^{-1}.C_G) * X_\omega = \omega^2.X_\omega \tag{B.2}$$

Replacing ω^2 by λ and E by $(I_G + A_G)^{-1}.C_G$ in (B.2) leads to the typical eigenvalue problem:

$$E * X_\omega = \lambda.X_\omega \tag{B.3}$$

This equation is solved by looking for the values of λ_n for which the determinant of $|E - \lambda\ .\ \mathbb{I}|$ is null ($\mathbb{I}$ being the identity matrix). The natural oscillation modes of the systems are defined by the eigen frequencies ω_n and the corresponding eigen modes X_{ω_n}.